6840 *Inorg. Chem.* **2010**, *49*, 6840–6852
DOI: 10.1021/ic100202h

Inorganic Chemistry
Article

Effects of Electronic Mixing in Ruthenium(II) Complexes with Two Equivalent Acceptor Ligands. Spectroscopic, Electrochemical, and Computational Studies

Marco M. Allard,[†] Onduru. S. Odongo,[†] Mandy M. Lee,[‡] Yuan-Jang Chen,*[,‡] John F. Endicott,*[,†] and H. Bernhard Schlegel*[,†]

[†]*Department of Chemistry, Wayne State University, Detroit, Michigan 48202, and*
[‡]*Department of Chemistry, Fu Jen Catholic University, Taipei Hsien 24205, Taiwan, R. O. C.*

Received February 1, 2010

The lowest energy metal to ligand charge transfer (MLCT) absorption bands found in ambient solutions of $[Ru(NH_3)_4(Y\text{-}py)_2]^{2+}$ and $[Ru(L)_2(bpy)_2]^{+}$ complexes (Y-py a pyridine ligand and $(L)_n$ a substituted acetonylacetonate, halide, am(m)ine, etc.) consist of two partly resolved absorption envelopes, $MLCT_{lo}$ and $MLCT_{hi}$. The lower energy absorption envelope, $MLCT_{lo}$, in these spectra has the larger amplitude for the bis-(Y-py) complexes, but the smaller amplitude for the bis-bpy the complexes. Time-dependent density functional theory (TD-DFT) approaches have been used to model 14 bis-bpy, three bis-(Y-py), and three mono-bpy complexes. The modeling indicates that the lowest unoccupied molecular orbital (LUMO) of each bis-(Y-py) complex corresponds to the antisymmetric combination of individual Y-py acceptor orbitals and that the transition involving the highest occupied molecular orbital (HOMO) and LUMO (HOMO→LUMO) is the dominant contribution to $MLCT_{lo}$ in this class of complexes. The LUMO of each bis-bpy complex that contains a C_2 symmetry axis also corresponds largely to the antisymmetric combination of individual ligand acceptor orbitals, while the LUMOs are more complex when there is no C_2 axis; furthermore, the energy difference between the HOMO→LUMO and HOMO→LUMO+1 transitions is too small (<1000 cm^{-1}) to resolve in the spectra of the bis-bpy complexes in ambient solutions. Relatively weak $MLCT_{lo}$ absorption contributions are found for all of the $[Ru(L)_2(bpy)_2]^{m+}$ complexes examined, but they are experimentally best defined in the spectra of the $(L)_2$ = X-acac complexes. TD-DFT modeling of the HOMO→LUMO transition of $[Ru(L)_4bpy]^{m+}$ complexes indicates that it is too weak to be detected and occurs at significantly lower energy (about 3000−5000 cm^{-1}) than the observed MLCT absorptions. Since the chemical properties of MLCT excited states are generally correlated with the HOMO and/or LUMO properties of the complexes, such very weak HOMO→LUMO transitions can complicate the use of spectroscopic information in their assessment. As an example, it is observed that the correlation lines between the absorption energy maxima and the differences in ground state oxidation and reduction potentials ($\Delta E_{1/2}$) have much smaller slopes for the bis-bpy than the mono-bpy complexes. However, the observed $MLCT_{lo}$ and the calculated HOMO→LUMO transitions of bis-bpy complexes correlate very similarly with $\Delta E_{1/2}$ and this indicates that it is the low energy and small amplitude component of the lowest energy MLCT absorption band that is most appropriately correlated with excited state chemistry, not the absorption maximum as is often assumed.

Introduction

The lowest energy electronic excited states of $[M(L)_{6-2n}(PP)_n]^{n+}$ complexes with polypyridyl ligands (PP) have long been useful as facile electron-transfer donors or acceptors in processes that range from bimolecular electron transfer reagents to dyes for solar photocells.[1−6] The electron-transfer reactivity of the metal to ligand charge transfer (MLCT) excited states of these complexes depend on the differences in their energies and molecular geometries from those of their ground states, but direct determinations of MLCT excited state energies and structures are generally very difficult and they are most often inferred from various kinds of spectroscopic measurements and various levels of computational modeling. In addition to these difficulties, the relationships between the inferred excited state properties

*To whom correspondence should be addressed. E-mail: 054971@mail.fju.edu.tw (Y.-J.C.), jfe@chem.wayne.edu (J.F.E.), hbs@chem.wayne.edu (H.B.S.).

(1) *Electron Transfer in Chemistry*; Balzani, V., Ed.; Wiley-VCH: Weinheim, Germany, 2001; Vol. *1*−*5*.
(2) Meyer, T. J.; Taube, H. In *Comprehensive Coordination Chemistry*; Wilkinson, G., Gillard, R. D., McCleverty, J., Eds.; Pergamon: Oxford, England, 1987; Vol. *7*; pp 331.
(3) Barbara, P. F.; Meyer, T. J.; Ratner, M. *J. Phys. Chem.* **1996**, *100*, 13148.
(4) O'Regan, B.; Graetzel, M. *Nature* **1991**, *353*, 737.
(5) Graetzel, M.; Moser, J.-E. In *Electron Transfer in Chemistry*; Balzani, V., Ed.; Wiley-VCH: Weinheim, 2001; Vol. *5*; pp 589.
(6) Graetzel, M. *Inorg. Chem.* **2005**, *44*, 6841.

 Published on Web 07/08/2010

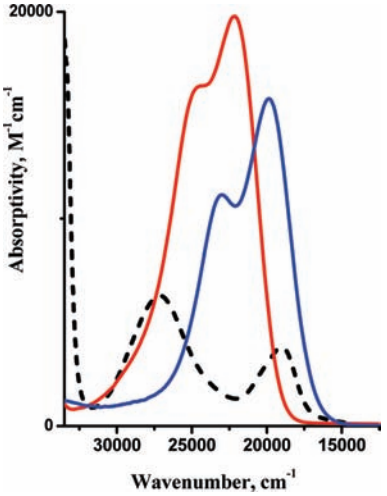

Figure 1. Lowest energy MLCT absorption bands in acetonitrile solutions of $[Ru(NH_3)_4bpy]^{2+}$ (dashed curve), *cis*-$[Ru(NH_3)_4(4\text{-phenyl-py})_2]^{2+}$ (red curve), and *cis*-$[Ru(NH_3)_4(4\text{-acetyl-py})_2]^{2+}$ (blue curve).

and their chemical reactivity are commonly based on perturbation theory models in which the electronic coupling (represented in terms of an effective matrix element H_{DA}) between the donor and acceptor is assumed to be weak ($|H_{DA}/E_{DA}|^2 < 0.1$)[1,2,7−11] whereas H_{DA} tends to be very large for Ru^{II}-polypyridyl complexes,[12−19] and the implications of the resulting effects of strong electronic coupling are poorly understood.[11]

The electron-transfer properties of simple complexes with a single metal donor (D) and two adjacent ligand acceptors, DA_2 complexes, can be further modified by the electronic mixing between acceptors (i.e., the mixing between the diabatic electronic excited states in which the electron is promoted to different acceptors: $\{A.A^-\}$ or $\{A^-.A\}$), and it is important to distinguish the limits (a) in which the A/A^- mixing is small and the acceptors are largely independent from that (b) in which the acceptors are very strongly mixed and are most meaningfully treated as a single (acceptor) entity, effectively a DA complex. In the context of this report, *cis*-$[Ru(NH_3)_4(Y\text{-py})_2]^{2+}$ and $[Ru(NH_3)_4bpy]^{2+}$, respectively, are plausible examples of these limits, and this difference can lead to marked contrasts in spectroscopic properties as illustrated in Figure 1, and very likely to related contrasts in excited state electron transfer properties.

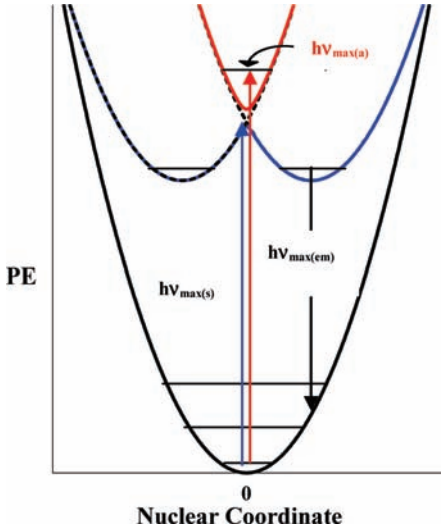

Figure 2. Qualitative potential energy (PE) diagram illustrating the relationships between the lowest energy MLCT singlet electronic states of a complex in the three state DA_2 limit when there is some configurational mixing between diabatic $MLCT_\alpha$ and $MLCT_\beta$ excited states. Two MLCT transitions are expected in this limit with $h\nu_{max(a)} > h\nu_{max(s)}$.

Simple perturbation theory-based three state models,[20] such as schematically represented in Figure 2, are often used to interpret the overall features of MLCT absorption spectra of transition metal DA_2 complexes such as those in Figure 1.[15,21−23] In this approach the A/A^- interaction in the MLCT excited state is somewhat analogous to the Hush approach to the properties of ground state mixed valence species,[7,8,11,17,24,25] but with the metal (D^+) mediating the ("superexchange") coupling between A and A^- in the MLCT excited state. However, the ambient absorptions of Ru(II) complexes tend to be broad and structureless, as illustrated in Figure 1, and can contain several different electronic excited state origins with their respective vibronic sidebands.[26−28] In practice, the lowest "MLCT excited state" energies of such complexes are often based on the energy of the dominant observed ambient absorption maxima[29−31] even though these absorption bands could be the convolution of several MLCT components or that more weakly absorbing lower energy MLCT excited states may be more relevant.[32−36]

(7) Hush, N. S. *Prog. Inorg. Chem.* **1967**, *8*, 391.
(8) Hush, N. S. In *Mechanistic Aspects of Inorganic Reactions*; Rorabacher, D. B., Endicott, J. F., Eds.; ACS Symposium Series 198; American Chemical Society: Washington, DC, 1982; p 301.
(9) Marcus, R. A. *Discuss. Faraday Soc.* **1960**, *29*, 21.
(10) Marcus, R. A. *Annu. Rev. Phys. Chem.* **1964**, *15*, 155.
(11) Endicott, J. F. In *Comprehensive Coordination Chemistry II*, 2 ed.; McCleverty, J., Meyer, T. J., Eds.; Pergamon: Oxford, U.K., 2003; Vol. *7*; p 657.
(12) Creutz, C.; Chou, M. H. *Inorg. Chem.* **1987**, *26*, 2995.
(13) Oh, D. H.; Boxer, S. G. *J. Am. Chem. Soc.* **1990**, *112*, 8161.
(14) Oh, D. H.; Sano, M.; Boxer, S. G. *J. Am. Chem. Soc.* **1991**, *113*, 6880.
(15) Seneviratne, D. S.; Uddin, M. J.; Swayambunathan, V.; Schlegel, H. B.; Endicott, J. F. *Inorg. Chem.* **2002**, *41*, 1502.
(16) Coe, B. J.; Harris, J. A.; Brunschwig, B. S.; I., A.; Clays, K.; Garin, J.; Orduna, J. *J. Am. Chem. Soc.* **2005**, *127*, 13399.
(17) Creutz, C.; Newton, M. D.; Sutin, N. *J. Photochem. Photobiol. A: Chem.* **1994**, *82*, 47.
(18) Crutchley, R. *Adv. Inorg. Chem.* **1994**, *41*, 273.
(19) Shin, Y. K.; Brunschwig, B. S.; Creutz, C.; Sutin, N. *J. Phys. Chem.* **1996**, *100*, 8157.
(20) Mulliken, R. S.; Person, W. B. *Molecular Complexes*; Wiley-Interscience: New York, 1967.
(21) Zwickel, A. M.; Creutz, C. *Inorg. Chem.* **1971**, *10*, 2395.
(22) Plummer, E. A.; Zink, J. I. *Inorg. Chem.* **2006**, *45*, 6556.
(23) Brunschwig, B. S.; Sutin, N. *Coord. Chem. Rev.* **1999**, *187*, 233.
(24) Hush, N. S. *Electrochim. Acta* **1968**, *13*, 1005.
(25) Creutz, C. *Prog. Inorg. Chem.* **1983**, *30*, 1.
(26) Yersin, H.; Braun, D.; Hensler, G.; Galhuber, E. In *Vibronic Processes in Inorganic Chemistry*; Flint, C. D., Ed.; Kluwer: Dordrecht, The Netherlands, 1989; p 195.
(27) Braun, D.; Hensler, C.; Gallhuber, E.; Yersin, H. *J. Phys. Chem.* **1991**, *95*, 1067.
(28) Lundqvist, M. J.; Galoppini, E.; Meyer, G. J.; Persson, P. *J. Phys. Chem. A* **2007**, *111*, 1487.
(29) Caspar, J. V.; Meyer, T. J. *Inorg. Chem.* **1983**, *22*, 2446.
(30) Lever, A. B. P.; Dodsworth, E. S. In *Electronic Structure and Spectroscopy of Inorganic Compounds*, Vol. *II*; Lever, A. B. P., Solomon, E. I., Eds.; Wiley: New York, 1999; p 227.
(31) Dodsworth, E. S.; Lever, A. B. P. *Chem. Phys. Lett.* **1986**, *124*, 152.
(32) Jorgensen, C. K. *Mol. Phys.* **1959**, *2*, 309.
(33) Jorgensen, C. K. *Orbitals in Atoms and Molecules*; Academic: New York, 1962.
(34) Bryant, G. M.; Ferguson, J. E.; Powell, H. K. *Aust. J. Chem.* **1971**, *24*, 257.
(35) Magnuson, R. H.; Taube, H. *J. Am. Chem. Soc.* **1975**, *97*, 5129.
(36) Kalinina, D.; Dares, C.; Kaluarachchi, H.; Potvin, P. G.; Lever, A. B. P. *Inorg. Chem.* **2008**, *47*, 10110.

This suggests that complexes that exhibit clear evidence of multiple electronic contributions within the observed lowest energy MLCT absorption band could be especially instructive. However, there are only a few pertinent reports and these are for complexes of the DA_2 class.[22,34,37−39] The most unequivocal of such reports are for the lowest energy MLCT absorption envelopes of the *cis*-$[Ru(NH_3)_4(Y\text{-}py)_2]^{2+}$ [22] and $[Ru(X\text{-}acac)(bpy)_2]^{+}$ [38,40] complexes for which the lowest energy MLCT absorption band is composed of two partially resolved low energy MLCT absorption envelopes with somewhat comparable amplitudes (e.g., see Figure 1).

Probably the most commonly used experimental basis for identifying MLCT transitions and evaluating their energies is the nearly 1:1 relationship expected between the absorption band energy maxima and the oxidation−reduction properties of the donor and acceptor moieties,[29−31,41,42]

$$h\nu_{max(MLCT)} = F\Delta E_{1/2} + \lambda + S \quad (1)$$

In this equation, λ is a nuclear reorganizational energy (containing both molecular and solvent contributions)[7,9,20] and S contains contributions from entropic, electrostatic, and other effects.[43] Equation 1 is based on simple models for the limit in which the donor and acceptor are weakly coupled and is well documented for the charge transfer spectra of ion pairs.[29−31,41,42,44] There is a potential problem in the application of eq 1 to systems in which the D−A electronic mixing is appreciable since as $\Delta E_{1/2} \rightarrow 0$ the reorganizational energy should also go to zero,[15,45,46] but there should still be an optical transition with significant absorption in this limit. Such an absorption is more similar to a $\pi\pi^*$[47] or a degenerate intervalence transition (IVT) than to a charge transfer transition. For example, the energies of IVTs approach $2H_{DA}$ in such a limit,[7] and this behavior is very well documented for many complexes.[2,11,18,25,39,44−46] In the classes of complexes considered here the effective H_{DA} has been estimated from electroabsorption studies to be about 10,500 cm^{-1} for Ru^{II}-py[48] and (based on a range of studies) about 7,000 cm^{-1} for Ru^{II}-bpy.[15,16] These estimates of H_{DA} are much larger than those for the Creutz−Taube ion (a paradigmatic IVT system with $300 < H_{DA}/cm^{-1} < 4000$),[18,25,49−51] and this suggests that there could be deviations from eq 1 in Ru^{II}-polypyridyl systems with $h\nu_{max(MLCT)} <$ ~15,000 cm^{-1}. The transition between the CT and non-CT regimes is likely to be gradual and could be obscured by the scatter when observations on many different classes of complexes are compared. In searching for such effects, we have compared the observations on complexes of the classes $[Ru(L)_2(bpy)_2]^{m+}$ and $[Ru(L)_4bpy]^{m+}$ for which $\Delta E_{1/2}$ can be varied over a 1 eV range by changes in the ancillary ligands L. The computational modeling of these systems indicates that several electronic origins do contribute to the observed absorption envelopes, that in many complexes the lowest energy MLCT transitions have oscillator strengths that are too small to be observed, and that the two low energy MLCT absorption envelopes found in DA_2 complexes with Ru(II) donors and nearly independent bipyridine or substituted pyridine acceptors involve contributions of transitions of different Ru(dπ) orbitals.

Experimental Section

A. Complexes and Reagents. The following commercial chemicals were used with no furthering purification: NH_4PF_6 and $[Ru(NH_3)_6]Cl_3$ (STREM); 4-phenylpyridine and 4-acetylpyridine (Aldrich). The complexes $[Ru(NH_3)_5Cl]Cl_2$, *cis*-$[Ru(NH_3)_4Cl_2]Cl$, $[Ru(NH_3)_5(H_2O)](PF_6)_2$, and *cis*- $[Ru(NH_3)_4(H_2O)_2](PF_6)_2$ were synthesized as described previously.[52] Literature syntheses were used for the $[Ru(NH_3)_5(4\text{-acetylpyridine})](PF_6)_2$, $[Ru(NH_3)_5(4\text{-phenylpyridine})](PF_6)_2$, *cis*-$[Ru(NH_3)_4(4\text{-acetylpyridine})_2](PF_6)_2$, $[Ru(CH_3CN)_4bpy](PF_6)_2$, and $[Ru(NH_3)_4bpy](PF_6)_2$.[22,53−57] The $[Ru(X\text{-}acac)_2bpy]$ and $[Ru(X\text{-}acac)(bpy)_2]^{+}$ complexes (X-ligand structures and abbreviations in Figure 3) were synthesized by variations of the procedures described by Dwyer, et al.[58,59] $[Ru(bpy)_2(tae)]PF_6$ and $[Ru(CH_3CN)_4bpy](PF_6)_2$ were prepared as described by Koiwa et al.[40] and Petroni et al.,[57] respectively. See Supporting Information S1 for further details.[60] Syntheses of most remaining complexes have been described previously.[38]

***cis*-$[Ru(NH_3)_4(ph\text{-}py)_2](PF_6)_2$.** A sample of *cis*-$[Ru(NH_3)_4(H_2O)_2](PF_6)_2$ (100 mg; 2 mmol) and 4-phenylpyridine (94 mg; 4.4 mmol) were combined with deaerated acetone (10 mL) and stirred in an argon atmosphere for approximately 2 h. After the solution color changed from light yellow to deep red, 100 mL of ether was slowly added to the reaction flask in an ice bath, and the orange product was removed by filtration. A 5 mL acetone solution of the initial product was added to an aqueous solution of 5 g of NH_4PF_6 (10 mL) cooled in an ice bath, and the orange precipitate was filtered, washed with 1 mL of cold water followed by cold ether (10 mL). The product was dried in vacuum oven. The yield was about 40%. Anal. Calcd. for $C_{22}H_{30}F_{12}N_6P_2Ru$: C, 34.34; H, 3.93; N, 10.92. Found: C,34.06; H, 4.19; N, 10.57. ^{1}1H-NMR(d_6-acetone): δ 2.62(6H), 3.17(6H), 7.57(6H), 7.68(4H), 7.77(4H), 8.63(4H). ^{13}C NMR(d_6-acetone): δ 123.18, 127.40, 130.28, 130.48, 137.38, 146.58, 157.89.

B. Instrumentation. UV−vis−NIR Absorption Spectra were determined using Shimadzu UV-2101PC or UV-3101PC spectrophotometers. Electrochemical measurements were performed using acetonitrile, butyronitrile, or dimethylformamide (DMF)

(37) Lever, A. B. P. *Inorganic Electronic Spectroscopy*; Elsevier: Amsterdam, The Netherlands, 1984.
(38) Odongo, O. S.; Heeg, M. J.; Chen, J. Y.; Xie, P.; Endicott, J. F. *Inorg. Chem.* **2008**, *47*, 7493.
(39) Koiwa, T.; Masuda, Y.; Shono, J.; Kawamoto, Y.; Hoshino, Y.; Hashimoto, T.; Natarajau, K.; Shimizu, K. *Inorg. Chem.* **2004**, *43*, 6215.
(40) Koiwa, T.; Masuda, Y.; Shono, J.; Kawamoto, Y.; Hoshino, Y.; Hashimoto, T.; Natarajau, K.; Shimizu, K. *Inorg. Chem.* **2004**, *43*, 6215.
(41) Gorelsky, S. I.; Kotov, V. Y.; Lever, A. B. P. *Inorg. Chem.* **1998**, *37*, 4584.
(42) Endicott, J. F. In *Electron Transfer in Chemistry*; Balzani, V., Ed.; Wiley-VCH: New York, 2001; Vol. *1*; pp 238.
(43) Richardson, D. E.; Taube, H. *Coord. Chem. Rev.* **1984**, *60*, 107.
(44) Cannon, R. D. *Adv. Inorg. Chem. Radiochem.* **1979**, *21*, 179.
(45) Matyushov, D. V.; Voth, G. A. *J. Phys. Chem. A* **2000**, *104*, 6470.
(46) Xie, P.; Chen, Y.-J.; Uddin, M. J.; Endicott, J. F. *J. Phys. Chem. A* **2005**, *109*, 4671.
(47) Ferretti, A.; Lami, A.; Villani, G. *Inorg. Chem.* **1998**, *37*, 2799.
(48) Shin, Y. K.; Szalda, D. J.; Brunschwig, B. S.; Creutz, C.; Sutin, N. *Inorg. Chem.* **1997**, *36*, 3190.
(49) Creutz, C.; Taube, H. *J. Am. Chem. Soc.* **1973**, *95*, 1086.
(50) Brunschwig, B. S.; Creutz, C.; Sutin, N. *Chem. Soc. Rev.* **2002**, *31*, 168.
(51) Demadis, K. D.; Hartshorn, C. M.; Meyer, T. *J. Chem. Rev.* **2001**, *101*, 2655.
(52) Krentzien, H. J., Ph.D dissertation, Stanford University, Palo Alto, CA, 1976.
(53) Durante, V. A.; Ford, P. C. *Inorg. Chem.* **1979**, *18*, 588.
(54) Pavanin, L. A.; da Rocha, Z. N.; Giesbrecht, E.; Tfouni, E. *Inorg. Chem.* **1991**, *30*, 2185.
(55) Ford, P. C.; Sutton, C. *Inorg. Chem.* **1969**, *8*, 1544.
(56) Curtis, J. C.; Sullivan, B. P.; Meyer, T. J. *Inorg. Chem.* **1983**, *22*, 224.
(57) Petroni, A.; Slep, L. D.; Etchenique, R. *Inorg. Chem.* **2008**, *47*, 951.
(58) Dwyer, F. P.; Goodwin, H. A.; Gyarfas, E. C. *Aust. J. Chem.* **1962**, *16*, 42.
(59) Dwyer, F. P.; Goodwin, H. A.; Gyarfas, E. C. *Aust. J. Chem.* **1963**, *16*, 544.
(60) See the Supporting Information.

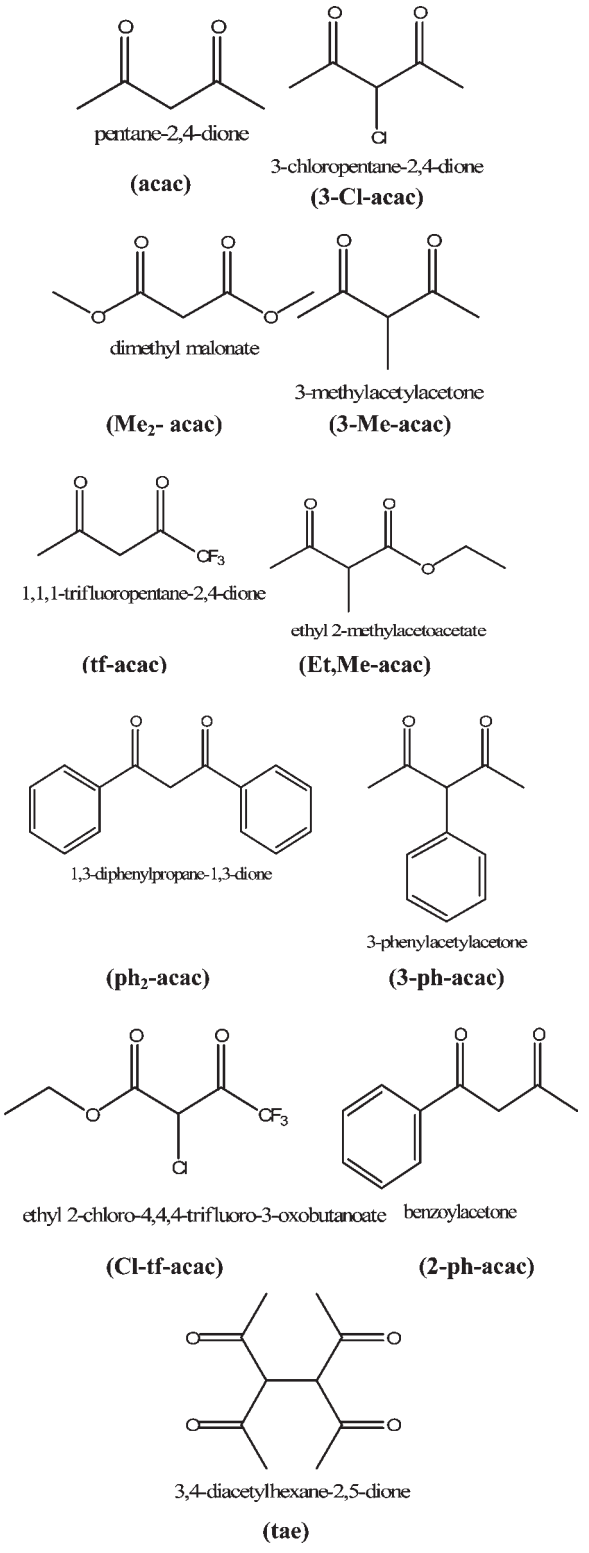

Figure 3. Skeletal structures and names (abbreviations in parentheses) for the X-acac ligands used in this work.

solvents, tetrabutylammonium hexafluorophosphate electrolyte, and a BAS 100B electrochemical system with either acetonitrile (AN) or butyronitrile solvents and tetrabutylyammonium hexafluorophosphate electrolyte. ^{1}H and ^{13}C NMR spectra were obtained using a Varian 300 MHz instrument.

C. Observed MLCT Absorption Envelopes. Deconvolutions of the lowest energy observed MLCT absorption bands were performed using either the Grams32 (as in Figure 4) or Origin 7

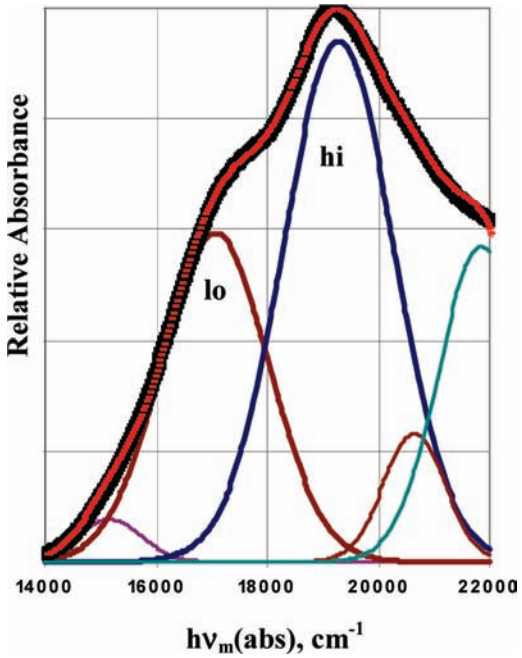

Figure 4. Lowest energy MLCT absorption band (heavy black curve) and Grams32 fit (thick red curve) for $[Ru(3\text{-Me-acac})(bpy)_2]^+$ in acetonitrile. The dominant MLCT absorption features are fitted with Gaussian bandshapes (dark red and dark blue curves); the other Gaussian features are introduced to optimize the fit for the contributions of $MLCT_{lo}$ and $MLCT_{hi}$ absorption envelopes.

programs, assuming that the lowest energy band is composed of two dominant contributions; the lower and higher energy experimental MLCT absorption envelopes are labeled $MLCT_{lo}$ and $MLCT_{hi}$, respectively. The observed absorption spectra, I_{obsd}, have been deconvoluted without the frequency correction ($I_{corr} = I_{obsd} \times \nu_m$)[61] for most of these complexes. This correction may make about a 5% difference in the ($h\nu_{II} - h\nu_{I}$) values in Table 1, but this is within the estimated deconvolution and experimental uncertainties. It is important to note that the Gaussian deconvolutions that we have used do not include any estimate of the vibronic sideband contributions while resonance-Raman spectra indicate that these constitute very appreciable contributions to the absorption spectra (see Supporting Information S2).[60,62,63] We estimate the uncertainties in deconvolution of the dominant observed MLCT peak energy to be about ±0.5%, but since the $MLCT_{lo}$ and $MLCT_{hi}$ peaks are not well separated and the vibronic sidebands are not considered (see Supporting Information Figure S2)[60] the uncertainties in the $MLCT_{hi}$ maxima are larger: the effects of neglecting the overlap with vibronic components from $MLCT_{lo}$ will lead to an underestimate of the $MLCT_{hi}$ energy while the neglect of its vibronic contributions will result in an overestimate of this energy. The $MLCT_{lo}$ absorption envelopes of the other $[Ru(L)_2(bpy)_2]^{m+}$ complexes are relatively weak, and the uncertainties in their deconvolutions are correspondingly large. In contrast, the (frequency corrected) energy differences between the $MLCT_{lo}$ and $MLCT_{hi}$ spectral absorption envelopes of the $[Ru(X\text{-py})(bpy)_2]^{2+}$ complexes are about 50% greater than those of the $[Ru(X\text{-acac})(bpy)_2]^+$ complexes, and this results in appreciably less uncertainty in their deconvolution.

D. Computational Techniques. Electronic structure calculations were carried out with the Gaussian 09 suite of programs[64]

(61) Gould, I. R.; Noukakis, D.; Gomez-Jahn, L.; Young, R. H.; Goodman, J. L.; Farid, S. *Chem. Phys.* **1993**, *176*, 439.
(62) Hupp, J. T.; Williams, R. T. *Acc. Chem. Res.* **2001**, *34*, 808.
(63) Maruszewski, K.; Bajdor, K.; Strommen, D. P.; Kincaid, J. R. *J. Phys. Chem.* **1995**, *99*, 6286.

Table 1. Lowest Energy MLCT Absorption Envelopes Found for Some $[Ru(L)_{6-2n}(bpy)_n]^{m+}$ Complexes[a]

$(L)_2$	$h\nu_{max}(MLCT_{lo})$[b]	$h\nu_{max}(MLCT_{hi})$[c]	$\Delta h\nu_{max}$[d]	$F\Delta E_{1/2}$[e]
3-Me-acac	17,060 (2260) [0.63]	19,280 (2230)	2,220	16,920
Me,Et-acac	17,110 (2040) [0.54]	19,090 (2280)	1,980	17,070
3-ph-acac	17,200 (2060) [0.54]	19,380 (2500)	2,180	17,290
Me_2-acac	17,350 (2070) [0.66]	19,307 (2100)	1,960	17,280
acac	17,380 (1870) [0.48]	19,420 (2390)	2,040	17,580
tae	17,540 (2020) [0.70]	19,450 (2010)	1910	17,580[f]
ph-acac	17,550 (2110) [0.48]	19,460 (2280)	1,910	17,600
ph_2-acac	17,640 (2290) [0.44]	20,060 (2868)	2,420	17,740
3-Cl-acac	17,890 (2040) [0.66]	19,760 (2070)	1,870	17,820
Cl,tf-acac	18,360 (2440) [0.67]	20,460 (2240)	2,100	18,950
tf-acac	18,540 (2030) [0.59]	20,500 (2170)	1,960	18,820
malonate	15,760 (2880) [0.30][g]	17,690 (2080)[g]	2,230	16,100[g]
CO_3^{2-}[h]	16,020 (2450) [0.22]	18,340 (2230)	2,310	irrc
oxalate	16,630 (2580) [0.24]	19,080 (2410)	2,450	16,210
$(Cl)_2$[h]	16,440 (2480) [0.24]	18,760 (2210)	2,320	~16,000
$(Br)_2$[h]	16,590 (2580) [0.16]	19,390 (2800)	2,800	~16,000
$(NH_3)_2$[i,j]	18,330 (2000) [0.20][f]	20,360 (1940)[f]	2,030	19,280[f]
(AN)(Br)[h]	19,140 (3340) [0.24]	21,230 (2530)	2,080	19,110
$(AN)_2$[h]	21,570 (2050) [0.20]	23,370 (1870)	1,800	24,110
(bpy)[i]	19,900 (2330) [0.10]	21,970 (1890)	2,070	21,000
$(NH_3)_4$[j]	16,650 (1631) [0.06][f]	18,850 (1914)[f]	2,200	18,100[f]
$(CH_3CN)_4$[k]	23,790 (3070) [0.17]	25,270 (2020)	1,480	24,910
$(acac)_2$[l]	14,280 (1830) [0.10]	16,100 (2063)	1,820	
$(acac)_2$[l]	14,150 (1750) [0.08][f]	16,140 (2190)[f]	1,990	15,810

[a] Energy maxima are based on Gaussian deconvolutions of the absorption envelopes (see Figure 4); ethanol/methanol solutions except as indicated; abbreviations as in Figure 3 (AN = acetonitrile). [b] Energies in cm^{-1} (full width at half height) [amplitude of $MLCT_{lo}$ absorption maximum relative to that of $MLCT_{hi}$]. The amplitudes are based on only a single MLCT contribution to the low energy shoulder, and they neglect vibronic contributions to the absorption spectra; since the latter tend to be quite large these ratios are probably lower limits. [c] Energies in cm^{-1} (full width at half height). [d] $\Delta h\nu_{max} = h\nu_{max(II)} - h\nu_{max(I)}$; energies in cm^{-1}. [e] Butyronitrile except as indicated; energies in cm^{-1}; F = Faraday's constant; irrc = irreversible cathodic wave. [f] Acetonitrile solvent. [g] DMF solvent. [h] Ref 38. [i] $[Ru(bpy)_3]^{2+}$.[84] [j] $[Ru(NH_3)_4bpy]^{2+}$.[84] [k] $[Ru(CH_3CN)_4bpy]^{2+}$. [l] $[Ru(acac)_2bpy]$.

using density functional theory (DFT). Calculations with the B3LYP[65] functional employed the LANL2DZ[66] basis set and pseudopotential, while calculations with the B3PW91[65,67−69] and LC-ωPBE[70,71] functionals used the SDDAll basis set.[72,73] A series of calculations was also carried out with a variety of larger basis sets (up to aug-cc-pVQZ on the ligands)[74] and the SDD pseudopotentials on the ruthenium metal center (see Supporting Information Table S3).[60] Since all of the ground states were closed shell singlets, calculations were carried out with spin restricted wave functions. Tight SCF convergence (10^{-8} for the rms density difference) was used throughout. The singlet ground state wave functions were checked for SCF stability,[75,76] and the lowest triplet states were calculated to ensure that they were higher in energy than the singlets. The geometries of all ground state structures were fully optimized, and vibrational frequencies were computed to confirm that the structures were energy minima.[77] Solvent effects in acetonitrile were estimated using the IEF-PCM polarizable continuum model.[78,79] Vertical electronic excitation energies and intensities were calculated by time-dependent density functional theory (TD-DFT).[80,81] Molecular orbitals were plotted with GaussView,[82] and UV−vis spectral plots were prepared using SWizard[83] with a full width at half-height of 2000 cm^{-1} (to facilitate both the evaluation of the convolution of near in energy components and the energies of the modeled absorption envelopes).

Results

A. Characteristics of the Absorption Spectra. The absorption spectra of the $[Ru(X\text{-}acac)(bpy)_2]^+$ and *cis*-$[Ru(NH_3)_4(Y\text{-}py)_2]^{2+}$ complexes examined in this study exhibit two well-defined, low energy MLCT absorption envelopes (see Figures 4 and 5 and Supporting Information Figure S4).[60] The amplitudes of the $MLCT_{hi}$ absorption envelopes are the largest for the former while the $MLCT_{lo}$ amplitudes are the largest for the latter complexes. The $[Ru(L)_2(bpy)_2]^{m+}$ complexes that we have examined for which $(L)_2$ is not an X-acac ligand exhibit much weaker lowest energy absorption features that we interpret as weak MLCT absorptions; see Figure 5 and Table 1. Since Ru(II) complexes always have weak low energy absorption features, some of which probably arise from spin−orbit-coupling allowed triplet absorptions, the resolved $MLCT_{lo}$ amplitudes are to be interpreted as upper limits. Although relatively weak, the low energy MLCT shoulder is well-defined for the $[Ru(Cl)_2(bpy)_2]^{2+}$ complex as was recognized long ago;[34,37] the resolved low energy absorption envelopes of the complexes with $(L)_2 \neq$ X-acac have between 15 and 25% of the dominant absorption envelope's amplitude. The similarly resolved (using Grams32) shoulders of the $[Ru(bpy)_3]^{2+}$ and $[Ru(NH_3)_4bpy]^{2+}$ MLCT absorption bands have more than about 5% but less than 20% of the intensity of the principal MLCT absorption envelope (Table 1). The energy difference between the $MLCT_{hi}$ and $MLCT_{lo}$

(64) Frisch, M. J.; Trucks, G. W.; Schlegel, H. B.; Scuseria, G. E.; Robb, M. A.; Cheeseman, J. R.; Scalmani, G.; Barone, V.; Mennucci, B.; Petersson, G. A.; Nakatsuji, H.; Caricato, M.; Li, X.; Hratchian, H. P.; Izmaylov, A. F.; Bloino, J.; Zheng, G.; Sonnenberg, J. L.; Hada, M.; Ehara, M.; Toyota, K.; Fukuda, R.; Hasegawa, J.; Ishida, M.; Nakajima, T.; Honda, Y.; Kitao, O.; Nakai, H.; Vreven, T.; Montgomery, J. A.; Peralta, J. E.; Ogliaro, F.; Bearpark, M.; Heyd, J.; Brothers, J. E.; Kudin, K. N.; Staroverov, V. N.; Kobayashi, R.; Normand, J.; Raghavachari, K.; Rendell, A.; Burant, J. C.; Iyengar, S. S.; Tomasi, J.; Cossi, M.; Rega, N.; Millam, J. M.; Klene, M.; Knox, J. E.; Cross, J. B.; Bakken, V.; Adamo, C.; Jaramillo, J.; Gomperts, R.; Stratmann, R. E.; Yazyev, O.; Austin, A. J.; Cammi, R.; Pomelli, C.; Ochterski, J. W.; Martin, R. L.; Morokuma, K.; Zakrzewski, V. G.; Voth, G. A.; Salvador, P.; Dannenberg, J. J.; Dapprich, S.; Parandekar, P. V.; Mayhall, N. J.; Daniels, A. D.; Farkas, O.; Foresman, J. B.; Ortiz, J. V.; Cioslowski, J.; Fox, D. J. *Gaussian G09*; Gaussian,Inc.: Wallingford, CT, 2009.
(65) Becke, A. D. *J. Chem. Phys.* **1993**, *98*, 5648.
(66) Dunning, T. H., Jr.; Hay, P. J. In *Modern Theoretical Chemistry*; Schaefer, H. F., III, Ed.; Plenum: New York, 1976; Vol. *3*; p 1.
(67) Krishnan, R.; Binkley, J. S.; Seeger, R.; Pople, J. A. *J. Chem. Phys.* **1980**, *72*, 650.
(68) Perdew, J. P. *Phys. Rev. B* **1986**, *33*, 8822.
(69) Perdew, J. P.; Burke, K.; Wang, Y. *Phys. Rev.* **1996**, *54*, 16533.
(70) Tawada, Y.; Tsuneda, T.; Yanagisawa, S.; Yanai, T.; Hirao, K. *J. Chem. Phys.* **2004**, *120*, 8425.
(71) Vydrov, O. A.; Scuseria, G. E.; Perdew, J. P. *J. Chem. Phys.* **2007**, *126*, 154109.
(72) Dunning, T. H., Jr.; Hay, P. J. In *Modern theoretical Chemistry*; Schaefer, H. F., III, Ed.; Plenum: New York, 1976; Vol. *3*; pp 1.
(73) Leininger, T.; Nicklass, A.; Stoll, H.; Dolg, M.; Schwerdtfeger, P. *J. Chem. Phys.* **1996**, *105*, 1052.
(74) Woon, D. E.; Dunning, T. H., Jr. *J. Chem. Phys.* **1993**, *98*, 1358.
(75) Schlegel, H. B.; McDouall, J. J. In *Computational Advances in Organic Chemistry*; Ögretir, C., Csizmadia, I. G., Eds.; Kluwer Academic: Amsterdam, The Netherlands, 1991.
(76) Bauernschmitt, R.; Ahlrichs, R. *J. Chem. Phys.* **1996**, *104*, 9047.
(77) Schlegel, H. B. *J. Comput. Chem.* **1982**, *3*, 214.
(78) Miertuš, S.; Scrocco, E.; Tomasi, J. *Chem. Phys.* **1981**, *55*, 117.
(79) Tomasi, J.; Mennucci, B.; Cammi, R. *Chem. Rev.* **2005**, *105*, 2999.
(80) Vlcek, A., Jr.; Zális, S. *Coord. Chem. Rev.* **2007**, *251*, 258.
(81) Runge, E.; Gross, E. K. U. *Phys. Rev. Lett.* **1984**, *52*, 997.
(82) *GaussView* 5.08; Gaussian Inc.: Wallingford, CT, 2009
(83) Gorelsky, S. I. *SWizard program*, revision 4.6; http://www.sg-chem.net/, 2009.
(84) Chen, Y.-J.; Xie, P.; Heeg, M. J.; Endicott, J. F. *Inorg. Chem.* **2006**, *45*, 6282.

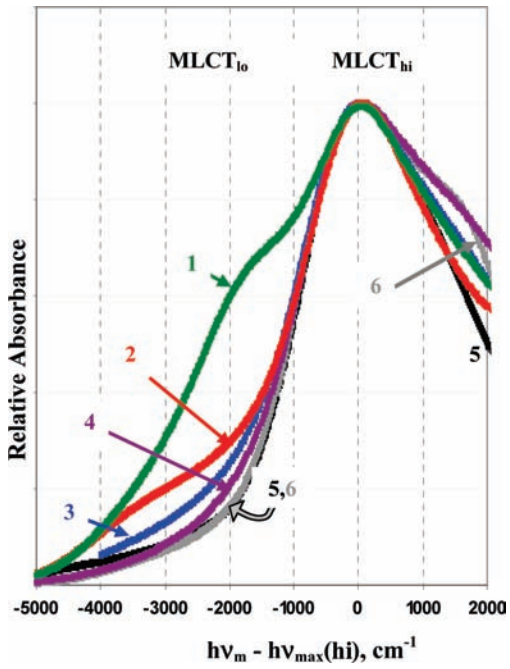

Figure 5. Lowest energy MLCT absorption region for [Ru(acac)-(bpy)$_2$]$^+$, 1; [Ru(Cl)$_2$(bpy)$_2$], 2; [Ru(NH$_3$)$_2$(bpy)$_2$]$^{2+}$, 3; [Ru(NCCH$_3$)$_2$-(bpy)$_2$]$^{2+}$, 4; [Ru(NH$_3$)$_4$bpy]$^{2+}$, 5; and [Ru(bpy)$_3$]$^{2+}$, 6. Complexes 1−3 show much more absorptivity in the MLCT$_{lo}$ region than do [Ru-(NH$_3$)$_4$bpy]$^{2+}$ and [Ru(bpy)$_3$]$^{2+}$. The absorption spectra (acetonitrile solutions) have been superimposed at their maxima in the MLCT$_{hi}$ region.

absorption envelopes of the bis-bpy complexes is approximately 2000 cm^{-1} (see Table 1) and appears to decrease with increasing energy of the MLCT transition (Figure 6).

We have used variations in the solvent to bring about shifts in MLCT energies for the [Ru(NH$_3$)$_4$(Y-py)$_2$]$^{2+}$ complexes; Figure 6 and Supporting Information Table S5.[60] The solvent dependent shifts were smaller (in solvents other than water) for the [Ru(L)$_2$(bpy)$_2$] complexes used in this study, and most of the energy variations for the bis-bpy complexes were the result of variations in their ancillary ligands; see Figure 6 and Supporting Information Table S6.[60] The energy differences between $h\nu_{max}$-(MLCT$_{hi}$) and $h\nu_{max}$(MLCT$_{lo}$) tend to decrease with increases of the MLCT energies for all of the bis-pyridyl and bis-bpy complexes examined independent of whether the excited state energies are varied by means of the "innocent" ligands or the solvent (Figure 6). These peak differences decrease as the transition energy increases for the *cis*-[Ru(NH$_3$)$_4$(Y-py)$_2$]$^{2+}$ which is the opposite of the trend expected for a simple three state model in which the lowest energy MLCT component corresponds to a symmetric A/A$^-$ combination (as implied by Figure 2) and mixes more strongly with the ground state than does the antisymmetric combination. The [Ru(L)$_2$(bpy)$_2$]$^{m+}$ complexes exhibit a similar pattern, while the energy differences between the well separated MLCT envelopes of the [Ru(NH$_3$)$_4$bpy]$^{2+}$ complex increase slightly as their energy increases (Figure 6).

B. Computational Results. Several combinations of density functionals and increasingly larger basis sets were explored (Supporting Information S8). The B3PW91 functional with the SDDALL basis set and pseudopotential and B3LYP/LANL2DZ gave the best agreement with

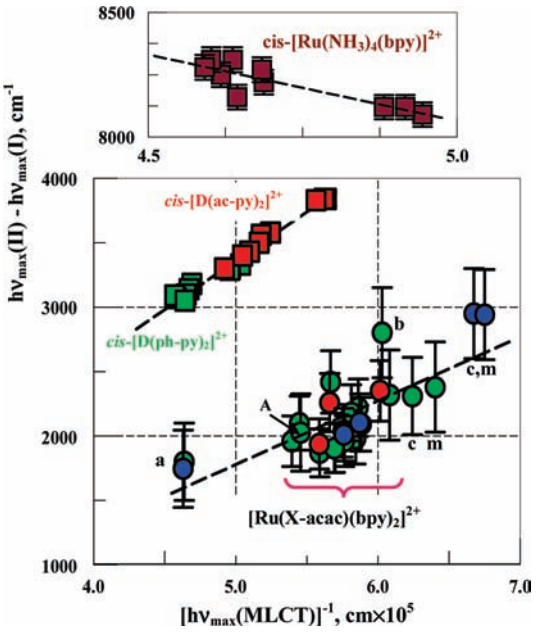

Figure 6. Correlation of the energy differences between the lowest energy MLCT absorption envelopes with the inverse transition energy for several bis-pyridyl and bis-bipyridyl complexes of Ru(II). The MLCT excited state energies of the *cis*-[Ru(NH$_3$)$_4$(Y-py)$_2$]$^{2+}$ (D = Ru(NH$_3$)$_4$; Y = phenyl or acetyl; green and red squares, respectively) and [Ru-(NH$_3$)$_4$bpy]$^{2+}$ (top panel) complexes have been modified by variations in the solvent, while those of the [Ru(L)$_2$(bpy)$_2$]$^{m+}$ complexes have been varied by altering the "spectator" ligand L in ethanol/methanol solvent (green circles) as well as the solvent. The latter series includes L = acetonitrile (a), (malonate; m)/2, Cl (c), Br (b), NH$_3$ (A) and several substituted acetylacetonates. Butyronitrile was also used as solvent for several complexes (blue circles), and some additional solvents were used for [Ru(3-Me-acac)(bpy)$_2$]$^+$ (red circles) . Note the expansion of the axes in the top panel. For the lower panel MLCT$_P$ = MLCT$_{lo}$; for the upper panel 2 $h\nu_{max}$-(MLCT$_P$) = $h\nu_{max}$(MLCT$_{lo}$) + $h\nu_{max}$(MLCT$_{hi}$)[1 − α^2_{gII}] where α_{gII} = H$_{ge}$/{$h\nu_{max}$(MLCT$_{av}$)[1 − H$^2_{ge}$/($h\nu_{max}$(MLCT$_{av}$))^2]$^{1/2}$}, H$_{ge}$ ~ 10,000 cm^{-1}, MLCT$_{av}$ ~ [MLCT$_{lo}$ + MLCT$_{hi}$(1 − α^2_{gII})]/2 and α^2_{gII} approximately accounts for the effects of configurational mixing with the ground state. The least-squares fits are [$\Delta h\nu$ = $h\nu_{max}$(II) − $h\nu_{max}$(I)]: 1. For [Ru(L)$_2$-(bpy)$_2$]$^{m+}$ (all complexes and all solvents): $\Delta h\nu$ = (5.3 ± 0.8) × 10^7-[$h\nu_{max}$(MLCT$_{lo}$)]$^{-1}$ − (0.5 ± 0.9) × 10^3 cm^{-1}; 2. For *cis*-[Ru(NH$_3$)$_4$(Y-py)$_2$]$^{2+}$: $\Delta h\nu$ = (7.6 ± 0.2) × 10^7[$h\nu_{max}$(MLCT$_{lo}$)]$^{-1}$ − (0.4 ± 0.1) × 10^3 cm^{-1}; 3. For Ru(NH$_3$)$_4$(bpy)]$^{2+}$: $\Delta h\nu$ = −(5 ± 1) × 10^7[$h\nu_{max}$-(MLCT$_{lo}$)]$^{-1}$ + (10.7 ± 0.5) × 10^3 cm^{-1}.

the observed results, and we have used the former to calculate electronic structures for 14 [Ru(L)$_2$(bpy)$_2$]$^{m+}$, 3 [Ru(L)$_4$bpy]$^{m+}$, and 3 [RuNH$_3$)$_4$(Y-py)$_2$]$^{2+}$ complexes (Supporting Information S10−S15).[60] The LC-ωPBE functional was developed to correct for systematic errors in charge transfer excitations.[70,71] However, with the default parameters, it overestimated the transition energies by as much as 7000 cm^{-1}. We did not observe significant ordering differences of the frontier orbitals, between solvated and gas phase calculations, despite typical shifts of ~40 cm^{-1} in absolute energy of the orbitals (see Supporting Information S9).[60] The PCM solvation methods resulted in transition energies that agreed better with observations than did the gas phase calculations. While the calculated orbital compositions were not greatly affected by including solvent, there were some small changes in the amount of ligand character in the frontier orbitals, most likely because of polarization effects of the solvent (see Supporting Information S9).[60]

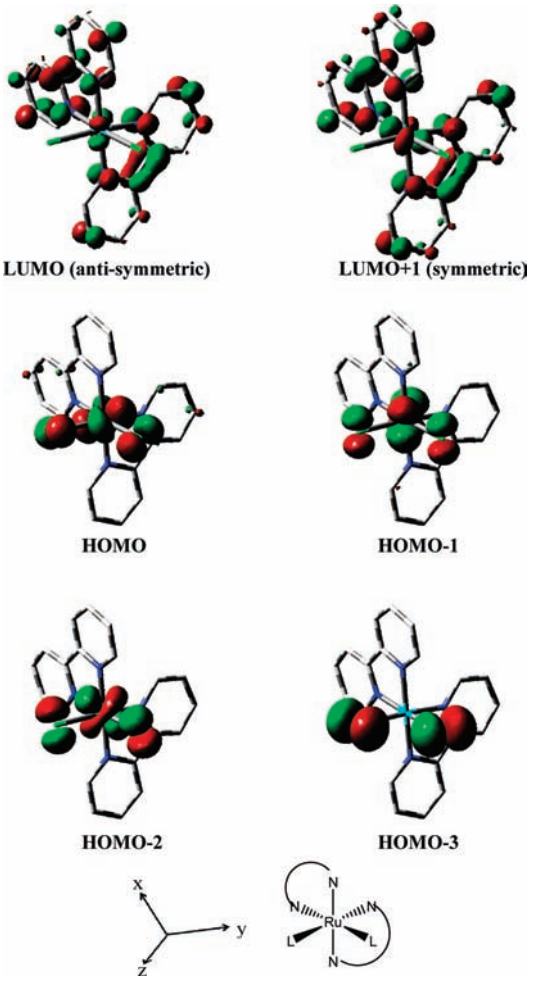

Figure 7. Orbitals for $[Ru(Cl)_2(bpy)_2]^{2+}$ calculated with B3PW91/SDDALL in acetonitrile. Note that all HOMOs contain Cl- and bpy-ligand contributions while LUMO and LUMO+1 contain different Ru-(dπ) contributions but negligible Cl contributions. Hydrogen atoms are omitted for clarity. The "symmetric" and "antisymmetric" notation refers to the combinations of independent bpy ligand LUMOs with respect to the C_2-axis (A and B representations, respectively, in the C_2 point group).

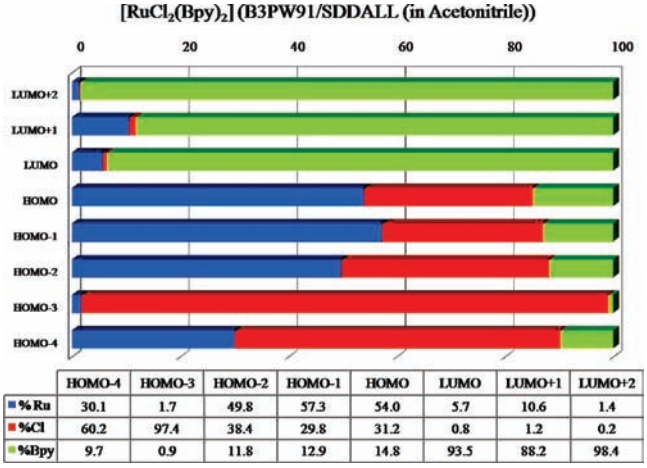

	HOMO-4	HOMO-3	HOMO-2	HOMO-1	HOMO	LUMO	LUMO+1	LUMO+2
%Ru	30.1	1.7	49.8	57.3	54.0	5.7	10.6	1.4
%Cl	60.2	97.4	38.4	29.8	31.2	0.8	1.2	0.2
%Bpy	9.7	0.9	11.8	12.9	14.8	93.5	88.2	98.4

Figure 8. Percent composition of frontier orbitals for $[Ru(Cl)_2(bpy)_2]$.

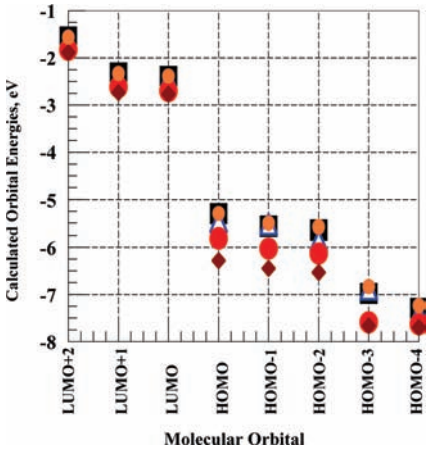

Figure 9. Comparison of highest occupied and lowest unoccupied molecular orbitals of $[Ru(L)_2(bpy)_2]^{m+}$ complexes calculated with B3PW91/SDDALL in acetonitrile solution; $(L)_2 = (Cl^-)_2$, black squares; malonate, white triangles; $acac^-$, orange circles; $(NH_3)_2$, red circles; $(CH_3CN)_2$, dark red diamonds.

1. Nature of HOMO, HOMO-1, and HOMO-2 in $[Ru(L)_2(bpy)_2]^{m+}$ Complexes and General Molecular Orbital Description. The calculated MOs (see Figure 7 and Supporting Information S10−S12)[60] reflect the molecular symmetry. For the bis-bpy complexes with C_2 symmetry the dπ orbitals are more closely related to e_π and a_π orbitals of D_3 symmetry than to the t_{2g} orbitals typical of O_h symmetry. Thus, the metal centered component of the highest occupied molecular orbital (HOMO) of $[Ru(Cl)_2(bpy)_2]$ in Figure 8 resembles a traditional d_{yz}-orbital with its plane slightly rotated with respect to the L-Ru-L plane where the z-axis (the C_2 axis) bisects the L-Ru-L angle; similarly, the metal centered component of the HOMO-1 resembles a "d_{xz}-orbital". However, these molecular orbitals, especially in complexes with anionic ancillary ligands such as Cl^- (Figure 8) or $acac^-$ (Supporting Information S6)[60] contain appreciable ligand character. Using different functionals/basis sets resulted in similar general patterns of the mixtures of ligand/metal combinations for these MOs, but the numerical details differed some (Supporting Information S8).[60] The computational modeling of the bis-bpy complexes indicates that the energies of HOMO, HOMO-1, and HOMO-2 are altered more by changes of the ancillary ligands than are the energies of the lowest unoccupied molecular orbitals, LUMO and LUMO+1; Figure 9 and Supporting Information S12.[60] The energy differences between the HOMO, HOMO-1, and HOMO-2 molecular orbitals of $[Ru(Cl)_2(bpy)_2]$ and $[Ru(acac)(bpy)_2]^+$ can be viewed as results of 3-centered (L-Ru-L) anti-bonding/non-bonding interactions between the respective p-type orbitals of the anionic ligands and the dπ-orbitals of Ru(II); in the dichloro complex the Ru(dπ) orbitals make up roughly 50−60% and the Cl atoms 30−40% of the resulting MOs (Figure 8). The HOMO-3 orbitals computed for the $[Ru(Cl)_2(bpy)_2]$ and $[Ru(acac)(bpy)_2]^+$ complexes were predominately ancillary-ligand centered.

2. Nature of LUMO and LUMO+1 in $[Ru(L)_2(bpy)_2]^{m+}$ Complexes. The LUMO and LUMO+1 orbitals computed for the $[Ru(L)_2(bpy)_2]^{m+}$ complexes with C_2 symmetry are antisymmetric and symmetric combinations, respectively, and nearly degenerate for any given complex (see Figures 7 and 9 and Supporting Information S12).[60] The calculated orbitals contain significant mixtures of Ru(dπ) orbitals (see Figures 7, 10 and 11). These observations imply that the excited state adiabatic

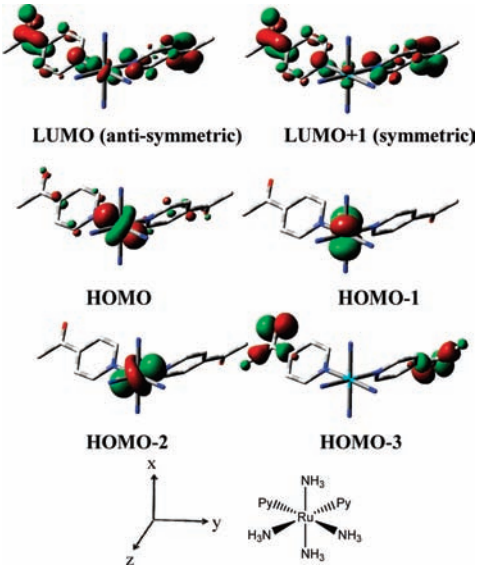

Figure 10. Orbitals computed for $[Ru(NH_3)_4(ac\text{-}py)_2]^{2+}$. Computational procedures as in Figure 7.

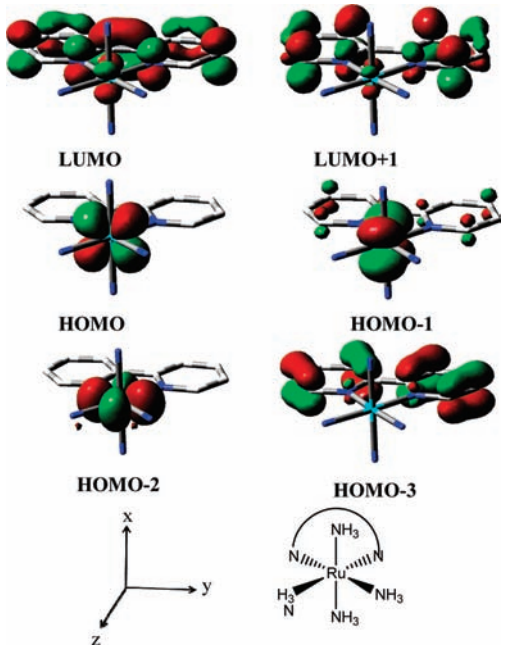

Figure 11. Orbitals computed for $[Ru(NH_3)_4(bpy)]^{2+}$. Computational procedures as in Figure 7.

surfaces in Figure 2 need to be modified to account for this metal-orbital mediated mixing with the symmetric and antisymmetric combinations of equivalent (diabatic) bpy ligand LUMOs in the DA_2 complexes, effectively doubling the number of PE surfaces with double minima.

The LUMO and LUMO+1 of the low symmetry (C_1) complexes do not correspond in a simple way to the symmetric and antisymmetric combinations of the related complexes with C_2 symmetry. Rather the orbital populations are unequally distributed over the acceptor ligands with their individual bpy-ligand population ratios varying from about 1:0.6 for $[Ru(tf\text{-}acac)(bpy)_2]^+$ to 1:0.2 for [Ru(malonate)$(bpy)_2$] (see Supporting Information S10).[60]

3. Orbitals of the *cis*-$[Ru(NH_3)_4(Y\text{-}py)_2]^{2+}$ and $[Ru(NH_3)_4bpy]^{2+}$ Complexes. The general patterns of the calculated HOMOs and LUMOs for the $[Ru(NH_3)_4(Y\text{-}py)_2]^{2+}$ complexes were similar to those described above for the $[Ru(L)_2(bpy)_2]^{m+}$ complexes (see Figure 10 and Supporting Information S11),[60] with slightly larger energy differences between LUMO and LUMO+1 ($\sim$1030 $\pm$ 150 and $\sim$400 $\pm$ 200 cm^{-1}, respectively) and with the LUMO corresponding to the antisymmetric combination of equivalent Y-py ligand LUMOs. The complex symmetry is again C_2, but the planes of the Y-py rings appear to be better oriented for overlap with the Ru(dπ) orbitals (see Figure 10 and Supporting Information S11)[60] than is found for the $[Ru(NH_3)_4bpy]^{2+}$

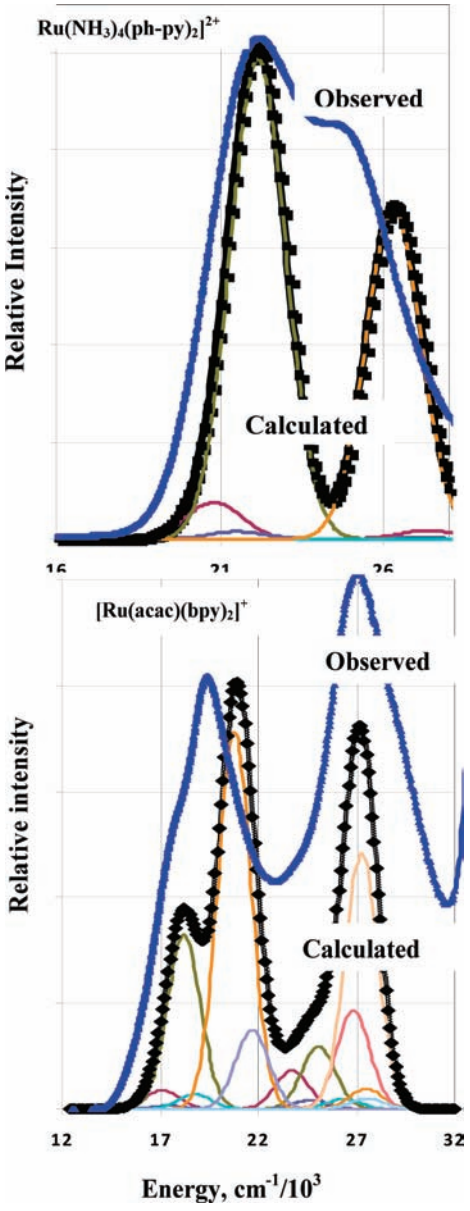

Figure 12. Comparison of the observed (thick blue lines) and calculated using B3PW91/SDDALL (dotted black lines) MLCT spectra of $[Ru(acac)(bpy)^+$ (lower panel; this includes $MLCT_{lo}$, $MLCT_{hi}$, and a higher energy MLCT envelope) and *cis*-$[Ru(NH_3)_4(ph\text{-}py)_2]^{2+}$ (upper panel; $MLCT_{lo}$ and $MLCT_{hi}$ only). The computed absorption envelopes were simulated using Gaussian bandshapes for the transition components (thin lines) with 2000 cm^{-1} full width at the half-height (fwhh) and the results of B3PW91/SDDALL calculations. The amplitudes of the calculated and observed spectra have been adjusted so that they are approximately equal for the dominant low energy MLCT absorption feature.

Table 2. Orbital Compositions of Calculated MLCT Transitions[a]

complex	$h\nu_{max}$ (obsd)[b] cm^{-1}	$h\nu_{max}$ (calc) cm^{-1}	f (calc)	assignment
$[Ru(Cl)_2(bpy)_2]$	16440	**16300**	**0.016**	**H-0→L+0(94%)**
		16700	0.0026	H-0→L+1(88%) H-2→L+1(8%)
		18400	0.0037	H-1→L+1(68%) H-2→L+0(29%)
		18900	0.0002	H-1→L+0(71%) H-2→L+1(27%)
	18790	**20200**	**0.15**	**H-2→L+0(66%) H-1→L+1(27%)**
		21500	0.014	H-2→L+1(57%) H-1→L+0(20%) H-0→L+1(9%) H-0→L(59%)
$[Ru(acac)(bpy)_2]^+$		17100	0.0065	H-0→L+0(75%) H-1→L+1(23%)
		17500	0.0012	H-0→L+1(74%) H-1→L+0(20%)
	17380	**18200**	**0.061**	**H-1→L+1(66%) H-0→L+0(18%) H-2→L+0(14%)**
		18800	0.0051	H-1→L+0(62%) H-2→L+1(27%) H-0→L+1(8%)
	19420	**20800**	**0.13**	**H-2→L+0(83%) H-1→L+1(9%) H-0→L+0(5%)**
		21700	0.028	H-2→L+1(62%) H-0→L+1(14%) H-1→L+0(13%) H-0→L+6(5%)
		23700	0.013	H-0→L+3(92%)
$[Ru(NH_3)_4bpy]^{2+}$		15500	0.0024	H-0→L+0(99%)
		17300	0.0000	H-2→L+0(98%)
	18850	**20500**	**0.049**	**H-1→L+0(87%) H-0→L+2(11%)**
		24500	0.015	H-0→L+1(96%)
	27120	**26000**	**0.013**	**H-0→L+2(53%) H-1→L+1(43%)**
		27800	**0.067**	**H-1→L+2(94%)**
		29500	0.15	H-1→L+1(53%) H-0→L+2(34%) H-1→L+0(9%)

[a] Using B3PW91/SDDALL with acetonitrile solvent parameters. The transitions in bold are assigned to the dominant contributions of the observed spectra. [b] See Table 1.

complex (Figure 11). In contrast to the bis-bpy and bis-(Y-py) complexes, the LUMO of $[Ru(NH_3)_4bpy]^{2+}$ corresponds to the symmetric combination of equivalent pyridyl moieties with respect to the C_2-axis.

4. Calculated and Observed Absorption Envelopes. The calculated and observed transition energies, and their relative intensities are compared for several complexes in Figure 12 and Supporting Information S14.[60] The notable general features of the computed MLCT absorption envelopes are as follows: (a) the calculated low energy absorption bands of the DA_2 complexes consist of two partly resolved absorption envelopes; (b) in most cases the observed $MLCT_{lo}$ and $MLCT_{hi}$ envelopes correspond to the convolution of more than one electronic transition (see Table 2 and Supporting Information S14 and S15);[60] (c) the energy differences between the electronic states of the $[Ru(L)_2(bpy)_2]^{m+}$ complexes that differ only in the contributions of LUMO or LUMO+1 are too small to be resolved in their observed absorption spectra; and (d) in many complexes there are apparently low energy MLCT transitions with oscillator strengths too small to be detected in solution spectra (Table 2 and Supporting Information S14 and S15).[60] The energies and bandshapes of the observed and calculated absorption bands are in good agreement as indicated in Figure 12 and Supporting Information S14.[60] Furthermore, the energy maxima calculated for two lowest energy MLCT absorption envelopes of the DA_2 complexes (based on transitions with relatively large calculated oscillator strengths) agree reasonably well with the energies of the experimental $MLCT_{lo}$ and $MLCT_{hi}$ absorption maxima (Figure 13); the intercept of the correlation in Figure 13 is systematically larger than expected (0), but it is very small compared to the uncertainties.

The computational studies on $[Ru(NH_3)_4(Y\text{-}py)_2]^{2+}$ complexes indicate that there are several contributions to the observed absorption bands in these complexes, but the dominant contributions to the $MLCT_{lo}$ and $MLCT_{hi}$ absorption envelopes are HOMO→LUMO (48−62%) and HOMO→LUMO+1 (69−71%), respectively; this contrasts to the $[Ru(L)_2(bpy)_2]^{m+}$ complexes for which the differences in band energies arise from the different energies of HOMO and HOMO-1. In addition there are (1) 3 or 4 lower energy transitions with very small oscillator strengths; (2) significantly larger energy differences (3000−4000 cm^{-1}) between the calculated and observed MLCT envelope maxima than the difference between the energies calculated for LUMO and LUMO+1 ($\sim 10^3$ cm^{-1}); and (3) appreciable HOMO-1 contributions to each of the transitions that have very large oscillator strengths.

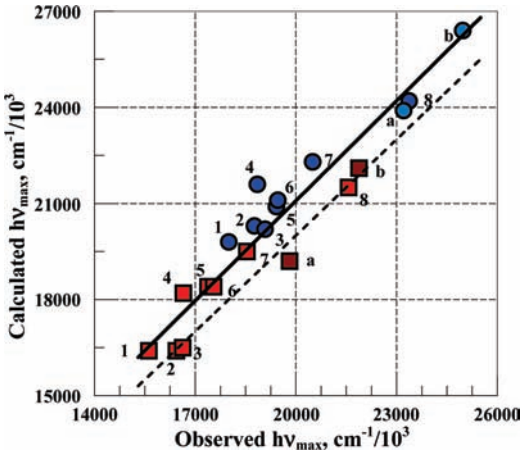

Figure 13. Comparison of $MLCT_{lo}$ and $MLCT_{hi}$ band maximum energies calculated (using B3PW91/SDDALL and acetonitrile parameters) to those observed for $[Ru(L)_n(A)_2]^{m+}$ complexes. The red squares are for $MLCT_{lo}$, and the blue circles are for the $MLCT_{hi}$ absorption envelopes of bis-bpy and bis-(Y-py) complexes. For the $[Ru(L)_2(bpy)_2]^{m+}$ complexes L = malonate/2 (1), Cl (2), oxalate/2 (3), NH_3 (4), acac/2 (5), 2-ph-acac/2 (6), tf-acac/2 (7), and CH_3CN (8). For the $[Ru(NH_3)_4(Y\text{-}py)_2]^{m+}$ complexes Y = acetyl (a) and phenyl (b). The dashed line is for a 1:1 correspondence between calculated and observed spectral maxima. For the solid least-squares line ($r^2 = 0.88$), $h\nu_{max}$(calcd) = $(1.04 \pm 0.10)h\nu_{max}$(obsd) + (300 ± 1900) cm^{-1}.

The spectral deconvolutions and the computational modeling (Figure 12 and Supporting Information S14

and S15)[60] indicate that two absorption envelopes are a characteristic feature of the lowest energy absorption band of the $[Ru(L)_2(bpy)_2]^{m+}$ class of complexes. Furthermore, the computational modeling for the bis-bpy complexes indicates that (a) the two absorption envelopes of their lowest energy MLCT bands arise largely from the differences in the energies of the HOMO and HOMO-1 donor orbitals; (b) the LUMO and LUMO+1 of the complexes with C_2 symmetry correspond to antisymmetric and symmetric combinations, respectively, of the individual diabatic bpy acceptor LUMOs; (c) $MLCT_{lo}$ is predominately a convolution of HOMO→LUMO and HOMO→LUMO+1 transitions (which are too similar in energy to be resolved in the ambient spectra); and (d) $MLCT_{hi}$ contains contributions that mostly involve HOMO-1 (and some HOMO-2). The lowest energy HOMO→LUMO and HOMO→LUMO+1 transitions calculated for $[Ru(X\text{-}acac)(bpy)_2]^+$ complexes have relatively small oscillator strengths and would not be easily resolved, but they are 50−300 cm^{-1} lower energy than the observed $MLCT_{lo}$ envelope maxima and about 10^3 cm^{-1} lower than the lowest energy calculated transitions with appreciable oscillator strengths (transitions involving HOMO-1). For the complexes with L = malonate/2, oxalate/2, NH_3, Cl, and CH_3CN, an appreciable oscillator strength is calculated for the HOMO→LUMO transition, and this corresponds well to $MLCT_{lo}$ while the contributions to $MLCT_{hi}$ arise mostly from HOMO-2→LUMO+n (n = 0−2) transitions.

The calculated oscillator strengths for the HOMO→LUMO transitions of the mono-bpy complexes are too small to observe in the experimental spectra. The calculations indicate that the observed low energy absorptions are 3000−5000 cm^{-1} higher energy and predominately HOMO-1→LUMO.

C. Spectroscopic-Electrochemical Correlations. The half-wave potentials for reduction of the $[Ru(X\text{-}acac)(bpy)_2]^+$ complexes average −1.42 ± 0.05 V (vs SSCE; Supporting Information Table S6) and most of the variations in $F\Delta E_{1/2}$ for the MLCT transitions from complex to complex arise from variations in $E_{1/2}(Ru^{III,II})$. The energies of both $MLCT_{lo}$ and $MLCT_{hi}$ correlate with the values of $F\Delta E_{1/2}$ as shown in Figure 7. Most of the MLCT absorption maxima for the $[Ru(L)_4bpy]^{m+}$ complexes, the $[Ru(X\text{-}acac)_2bpy]$ complexes reported here, and those for the tetraam(m)ine complexes reported previously[84] are mostly intermediate between the $MLCT_{lo}$ and $MLCT_{hi}$ maxima of $[Ru(L)_2(bpy)_2]^{m+}$ complexes with similar values of $F\Delta E_{1/2}$.

The least-squares fits for the $[Ru(X\text{-}acac)_2(bpy)_2]^+$ complexes shown in Figure 14 are (r^2 = 0.92 ± 0.03):

$$h\nu_{max}(MLCT_{lo}) = (0.73 \pm 0.05)F\Delta E_{1/2} + (4700 \pm 1000)\ cm^{-1} \quad (2)$$

and

$$h\nu_{max}(MLCT_{hi}) = (0.70 \pm 0.08)F\Delta E_{1/2} + (7200 \pm 1400)\ cm^{-1} \quad (3)$$

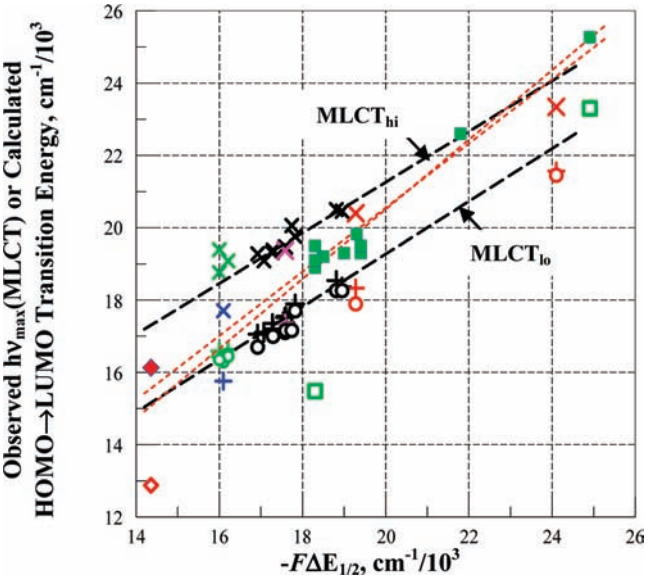

Figure 14. Correlation between the energies of MLCT absorption maxima and the differences between the half-wave potentials for oxidation and reduction of $[Ru(L)_2(bpy)_2]^{m+}$ and $[Ru(L)_4bpy]^{m+}$ complexes (F = Faraday's constant). The maxima of the observed Gaussian $MLCT_{lo}$ and $MLCT_{hi}$ absorption envelopes for $[Ru(L)_2(bpy)_2]^+$ complexes are designated by (+) and (×), respectively. Black and purple symbols are for the absorption spectra of the $[Ru(X\text{-}acac)(bpy)_2]^+$ complexes in methanol/ethanol or butyronitrile solvents, respectively; from left to right X-acac = 3-Me-acac, Me-Et-acac, Me_2-acac, 3-ph-acac, tae, acac, ph-acac, ph_2-acac, 3-Cl-acetone, tf-acac, and Cl, -tf-acac; For the other $[Ru(L)_2(bpy)_2]^{m+}$ complexes from left to right $(L)_2$: (a) red, $(NH_3)_2$ and $(CH_3CN)_2$ in acetonitrile (AN); (b) blue, malonate in methanol/ethanol; (c) green, malonate and oxalate in AN. Green squares are for the $[Ru(Am)_4bpy]^{2+}$ complexes (in AN); from[84] left to right $(Am)_4$ = $(NH_3)_4$ trien, [12]aneN$_4$, $(en)_2$, [15]aneN$_4$, pyo[14]eneN$_{4+}$, *rac*-[14]aneN$_4$, and Me_6[14]aneN$_4$, $(py)_4$; and, from this work, $(CH_3CN)_4$. Red diamonds are for $[Ru(acac)_2bpy]$ (in methanol/ethanol. The black dashed lines are least-squares fits of the respective $MLCT_{lo}$ and $MLCT_{hi}$ data points for the $[Ru(X\text{-}acac)_2(bpy)_2]^+$ complexes; the red short dashed lines are least-squares fits of the data points for the $[Ru(L)_4bpy]^{m+}$ complexes including or excluding the $[Ru(acac)_2bpy]$ point. The energies calculated for the HOMO→LUMO transitions are plotted as open circles for $[Ru(L)_2(bpy)_2]^{m+}$ complexes and as open squares or diamonds for the $[Ru(L)_4bpy]^{m+}$ complexes.

For the all of the $[Ru(L)_4bpy]^{m+}$ complexes (excluding the $[Ru(acac)_2bpy]$ point; r^2 = 0.96):

$$h\nu_{max}(MLCT) = (0.89 \pm 0.06)F\Delta E_{1/2} + (2800 \pm 1100)\ cm^{-1} \quad (4)$$

The least-squares lines that include all of the $MLCT_{lo}$ (or $MLCT_{hi}$) absorption spectral data in Figure 14 have somewhat more shallow slopes (ca. 0.6); the mono-bpy correlation based only on $[Ru(L)_4bpy]^{2+}$ complexes (black dashed line) has a slope of 0.96 ± 0.06 and intercept of about (1 ± 1) × 10^3 cm^{-1}. Thus, an overall correlation of all the complexes in Figure 14 with a unitary slope, as in eq 1, would correspond to $(\lambda + S) \sim (1 \pm 1) \times 10^3\ cm^{-1}$.

The oxidations and reductions of the complexes most likely involve the HOMO and the LUMO, respectively, and the transitions involving these orbitals should be the most relevant to $F\Delta E_{1/2}$. Since the lowest energy absorption maxima do not always correspond to such transitions, we have included the energies calculated for the HOMO→LUMO transitions in Figure 14. These calculated transitions

(and the calculated LUMO−HOMO energy differences; Supporting Information S17)[60] very closely follow the patterns of the observed $MLCT_{lo}$ maxima for the bis-bpy complexes. The very similar correlations of $E(MLCT_{lo})$ and $E(HOMO \rightarrow LUMO)$ with $F\Delta E_{1/2}$ in Figure 14 indicate that it is the lowest energy, smallest amplitude components of the low energy MLCT absorption band of bis-bpy complexes that are most relevant to spectroscopic/electrochemical correlations and not the generally used absorption maxima. However, the HOMO→LUMO transitions calculated for the mono-bpy complexes are a few thousand wavenumbers lower in energy than the observed MLCT band maxima for the mono-bpy complexes.

Discussion

The lowest energy MLCT absorption bands of the $[Ru(NH_3)_4(Y\text{-}py)_2]^{2+}$ and $[Ru(L)_2(bpy)_2]^{m+}$ classes of complexes are generally composed of two partly resolved absorption envelopes. Some general aspects of the assignment of these absorption envelopes can be based on experimental observations, but the assignments based on computational modeling are more detailed and decisive. These complexes can be considered to be of the DA_2 type since the A/A^- electronic mixing appears to be weak in both classes, and this contrasts to complexes of the $[Ru(L)_4bpy]^{m+}$ class in which the electronic mixing of the pyridyl moieties is so strong that the complexes are best considered to be of the DA type. The patterns of the orbital compositions differ from one class to another, and within each class the energies and the spatial orientations of the $Ru(d\pi)$ donor orbitals are modified by the ligands in ways that alter the observed patterns of absorption energies, absorptivities, and correlations of observed spectra with chemical behavior. The computational modeling leads to calculated lowest energy MLCT absorption bands whose energies and bandshapes are in reasonable accord with those observed for each class of complexes. The lowest energy MLCT absorption component of the bis-bpy complexes usually has a very small absorptivity and has been neglected in much previous work. The observations reported here indicate that it is this lowest energy component that is usually most relevant to the chemical properties of the MLCT excited states.

We have used the comparison of the electrochemical properties of the complexes to their lowest energy MLCT absorption components as an indication of how the contrasts in electronic structure inferred from the computational modeling might be manifested in the excited state chemical properties of the complexes. There are two notable contrasts in the comparisons of observed and calculated lowest energy electronic transition energies and the differences in oxidation and reduction potentials, $F\Delta E_{1/2}$, of the complexes: (a) for a given value of $F\Delta E_{1/2}$, the calculated HOMO→LUMO transitions are lower in energy for the mono- than for the bis-bpy complexes, but the difference appears to become smaller as the transition energy increases; (b) the observed and calculated slopes of the (transition energy)/$F\Delta E_{1/2}$ are appreciably more shallow for the bis- than for the mono-bpy complexes over the range of energies observed, with the latter approaching the unitary slope predicted by eq 1. These trends in the redox properties of the two classes of complexes can be addressed using classical perturbation theory arguments.

A. MLCT Spectra of DA_2 Complexes. 1. $[Ru(NH_3)_4(Y\text{-}py)_2]^{2+}$ Complexes. The orbital assignments indicate that the MLCT bands of the complexes with two independent pyridyl acceptors are better described by the three state perturbation theory model of Figure 2 than are those of the *bis*-bipyridyl complexes, but with the lowest energy MLCT excited states corresponding to the antisymmetric combinations of the diabatic pyridyl acceptor orbitals rather than with the symmetric combinations implicated in the figure and sometimes assumed.[22] In contrast, the two low energy MLCT absorption envelopes observed for bis-bpy complexes appear to correspond mostly to different donor orbital contributions. The antisymmetric assignment ($MLCT_a$) to the $MLCT_{lo}$ envelope of the bis-(Y-py) complexes is the one expected on the basis of three-state perturbation theory for the DA_2 limit, since in this limit only the symmetric $MLCT_s$ excited state would mix significantly with the ground state, and significant mixing could result in a larger energy for the symmetric state than for the antisymmetric state. Thus, decreases in overall excited state energies, with the concomitant increases in ground state/excited state mixing, would result in increasing differences in the energies of the $MLCT_s$ and $MLCT_a$ excited states as observed in Figure 6. The opposite pattern is expected in the limit that A/A^- mixing is very strong, and this is consistent with observations on $[Ru(NH_3)_4bpy]^{2+}$. Overall, the computational modeling supports the observations in Figure 6, and both the experimental and computational observations are consistent with weak and strong mixing of the pyridyl moieties of the $[Ru(NH_3)_4(Y\text{-}py)_2]^{2+}$ and $[Ru(NH_3)_4bpy]^{2+}$ complexes, respectively.

While the computational modeling is in reasonable agreement with perturbation theory in the assignment of $MLCT_{lo}$, it indicates that (a) the electronic excited states are much more numerous and complicated than assumed in a three state model; and (b) the symmetric and antisymmetric combinations of the $[Ru(NH_3)_4(Y\text{-}py)_2]^{2+}$ pyridyl ligands mix with orthogonal donor orbitals. A significant part of the complexity arises because there are three $Ru^{II}(d\pi)$ donor orbitals (in the diabatic limit) which have different symmetries and/or spatial distributions. However, this modeling also indicates that the observed $MLCT_{lo}$ and $MLCT_{hi}$ absorption envelopes are generally convolutions of several electronic transitions and that the transitions themselves are more complex than represented by a three state model.

2. Observations on $[Ru(L)_2(bpy)_2]^{m+}$ Complexes. The differences between the $MLCT_{lo}$ and $MLCT_{hi}$ absorption envelopes of the $[Ru(L)_2(bpy)_2]^{m+}$ complexes in Figure 6 parallel those for the $[Ru(NH_3)_4(Y\text{-}py)_2]^{2+}$ complexes, and the computational modeling of the bis-bpy complexes also indicates mixing of different donor orbitals with the symmetric and antisymmetric combinations of individual bpy LUMOs, consistent with the DA_2 limit. The computational modeling of these complexes also indicates that the HOMO→LUMO and HOMO→LUMO+1 transitions are similar enough in energy that both are often convoluted into the $MLCT_{lo}$ absorption envelope, and that the substantial differences between $MLCT_{hi}$ and $MLCT_{lo}$ absorption maxima in Table 1 and Figure 6 are largely the consequence of ligand-induced $d\pi$ orbital splittings and not the LUMO and LUMO+1

energy differences expected from three state perturbation theory models such as represented in Figure 2.

3. Implications of Observations on the $[Ru(L)_4bpy]^{m+}$ Complexes. Figure 11 suggests that only the C_2-adapted $\sim d_{xz}$ orbital has the spatial orientation for reasonable overlap with the pπ orbitals of the bpy ligand of $[Ru(NH_3)_4bpy]^{2+}$. Thus, only this metal dπ orbital is mixed significantly into both the LUMO and the LUMO+1 of this complex, in contrast to the mixing of different dπ orbitals with the symmetric and antisymmetric acceptor combinations found for the bis-(Y-py) and bis-bpy complexes. This very poor spatial overlap is very likely a major reason that the dominant transitions are those of HOMO-1 and that the lower energy transitions involving the HOMO have such small oscillator strengths. We find similar orbital properties for the $[Ru(acac)_2bpy]$ (Supporting Information S15)[60] and $[Ru(CH_3CN)_4bpy]^{2+}$ complexes (also noted previously for $[Ru(CH_3CN)_2bpy]^{2+}$).[57] This may be a feature common to mono-bpy complexes. This contrasts to the $[Ru(NH_3)_4(Y\text{-}py)_2]^{2+}$ complexes in which the angular disposition of pyridyl moieties in the bis-(Y-py) complexes probably leads to better LUMO spatial overlap with the Ru(dπ) orbitals and may account for greater absorptivities of the observed MLCT absorption bands of these complexes than their bpy analogue (Figure 1).

B. Correlations between Electronic Transition Energies and $F\Delta E_{1/2}$ for $[Ru(L)_4bpy]^{n+}$ and $[Ru(L)_2(bpy)_2]^{m+}$ Complexes. The observations summarized in Figure 14 indicate that the spectroscopic/electrochemical correlations are markedly different for the mono-bpy and bis-bpy complexes: (1) different correlation lines are found for each class of complexes for either the observed or the calculated transitions; and (2) the correlation lines for $MLCT_{lo}$ and $MLCT_{hi}$ of the bis-bpy complexes nearly bracket the mono bpy correlation, but with a slope of about 0.7 for both the $MLCT_{lo}$ and the $MLCT_{hi}$ correlations compared to about 0.9 for all the mono-bpy complexes considered.

In an idealized weak coupling limit $|F\Delta E_{1/2}|$ is an estimate of the energy difference between the ground and excited state energy minima ($E_d^{0'0}$), and in this limit configurational mixing is expected to contribute approximately equally to $F\Delta E_{1/2}$ and to the energy of the HOMO→LUMO transition of DA complexes. However, this is not necessarily the case for DA_2 complexes since there is still some D/A mixing when the reduction involves only one of the acceptor ligand moieties and the DA_2 equivalent of eq 1, ignoring any A/A^- mixing, is (see Supporting Information S17),[60]

$$h\nu_{max(H/L)} \approx -F\Delta E_{1/2} + \lambda_b + S + \varepsilon_{DA} \qquad (5)$$

where $\varepsilon_{DA} \approx H_{DA}^2/[(E_d^v)(1 + (H_{DA}/E_d^v)^2)] = \alpha_{DA}^2 E_d^v$ is the effective stabilization energy[20] that results from D/A configurational mixing, and $E_d^v \approx (E_d^{0'0} + \lambda_b)$ is the vertical energy difference between the diabatic ground and excited states. For a given value of $F\Delta E_{1/2}$, the ε_{DA} term in eq 5 would result in larger energy for the HOMO→LUMO transition in the bis- than in the mono-bpy complexes, and this difference should decrease as E_d^v increases, consistent with the calculated energies in Figure 14. It is also likely that the reorganizational energy contributions (λ and λ_b, respectively) will be different for the mono- and bis-bpy complexes. Thus, most of the attenuation of λ arises from the reduced distortion (represented as a displacement of $+2\alpha_{DA}^2 x_o$ and $-2\alpha_{DA}^2 x_o$ respectively for the ground and excited state PE minima) that arises as a result of configurational mixing, and in the limit of a single distortion coordinate (x_o) that is displaced in opposite directions for mixing with the individual acceptor ligands the net displacement of the ground state PE minimum is expected to be relatively small (i.e., $(2\alpha_{DA}^2 x_o - 2\alpha_{DA}^2 x_o) = 0$;[85] see Figure 2) and λ_b is expected to be larger than λ; this should result in larger HOMO→LUMO energy differences for the mono-bpy complexes, but in these non-linear systems with multiple displacement coordinates[26,62,63] this contribution is probably small.

The more shallow slopes found for the bis-bpy than mono-bpy complexes might be attributed to systematic variations in (a) some unique physical properties of the bis-bpy complexes; (b) the contributions of transitions of different orbital character to the spectroscopic transitions through the series of bis-bpy complexes; (c) the different effects of D/A (or $D/(A)_2$) configurational mixing with variations in the MLCT excited state/ground state energies. However, since the slopes of the bis-bpy correlation lines in Figure 7 are based on the $[Ru(X\text{-}acac)(bpy)_2]^+$ complexes but also correlate well with observations on the other $[Ru(L)_2(bpy)_2]^{m+}$ complexes and with the calculated HOMO→LUMO transition energies, it is very unlikely that there is a simple physical property (such as differences in charge, dipole, etc.) or differences in orbital character that can be the origin of the shallow slopes in Figure 14. Since configurational mixing increases as the ground state/MLCT excited state energy difference (or $h\nu_{max(d)}$) decreases, and since this energy difference does vary appreciably through the complexes included in Figure 14, a systematic variation in the extent of configurational mixing is a likely origin of the shallow slopes. With reference to eqs 1 and 5, such effects can arise from (a) attenuation of reorganizational energies (λ and λ_b) as the excited state energies decrease; and/or (b) a decrease in the amount of charge transfer character as E_d^v decreases.

Previous work has found decreases in emission sideband amplitudes with decreases in $h\nu_{max}$ for many of these complexes, and the implicated variations in excited state distortions are one consequence of appreciable configurational mixing.[38,46,84,86−88] This effect of configurational mixing can be expressed as an attenuation of the effective reorganizational energies (for $\alpha_{DA}^2 < 0.1$)

$$\lambda = \lambda^o(1 - n_{DA}\alpha_{DA}^2 + ...) \qquad (6)$$

where for the simplest limit (equal shifts of the ground and excited state PE minima and little difference in α_{DA}^2 for the coordinates of the respective PE minima) $n_{DA} \sim 4$.[38,46,84,86−88] Such attenuation of reorganizational

(85) Chen, Y.-J.; Endicott, J. F.; Swayambunathan, V. *Chem. Phys.* **2006**, *326*, 79.
(86) Matyushov, D. V.; Newton, M. D. *J. Phys. Chem. A* **2001**, *105*, 8516.
(87) Endicott, J. F.; Chen, Y.-J. *Coord. Chem. Rev.* **2007**, *251*, 328.
(88) Endicott, J. F.; Chen, Y.-J.; Xie, P. *Coord. Chem. Rev.* **2005**, *249*, 343.

energies would tend to increase, not decrease, the slopes of the correlations in Figure 14.

Thus, the shallow slopes of the correlations in Figure 14 probably arise because substantial ground state/excited state configurational mixing implies that $h\nu_{ge}$ will not approach zero when $-F\Delta E_{1/2} \rightarrow 0$. Rather, as the systems approach this limit the spectroscopic transitions have an increasing amount of character that is more analogous to that of a $\pi\pi^*$ than to a CT transition (i.e., $(DA_2) \rightarrow (DA_2)^*$ rather than $(DA_2) \rightarrow (D^+(A^-)(A))$.[47] For the two-state limit of a DA system the transition energy can be expressed as

$$h\nu_{max(H/L)} \approx [(E_d^v)^2 + 4H_{DA}^2]^{1/2} \quad (7)$$

When $E_d^v \gg 2|H_{DA}|$, then

$$h\nu_{max(H/L)} \sim E_d^v + 2\varepsilon_{DA} \quad (8)$$

Thus, D/A configurational mixing has the effect of adding a stabilization energy term to eq 1 and thereby decreasing the slopes of the spectroscopic/electrochemical correlations. This effect should be very approximately twice as large for a specific value of E_d^v in a DA_2 system. Furthermore, eq 7 implies that when $-F\Delta E_{1/2} \rightarrow 0$, the transition energy should approach a limiting value ($\sim 2H_{DA}$). We have not yet found bis-bpy complexes with sufficiently low energy MLCT absorbances to explore this limit, but the related limiting values have very recently been found to be more strongly implicated in the emission spectra of these complexes (note that for these systems $[h\nu_{max}(abs) - h\nu_{max}(emis)] \sim (3-5) \times 10^3\ cm^{-1}$).[89]

Conclusions

While a simple perturbation theory model which ignores the details of the donor and acceptor orbitals adequately represents the relationship between the charge transfer spectra and electrochemical properties of ion pairs, the detailed properties of these orbitals can complicate such relationships when the donor and acceptor are covalently linked. Nevertheless, the global perspective of perturbation theory can usefully complement the detailed information provided by DFT computational studies. Thus, the partly resolved absorption envelopes ($MLCT_{lo}$ and $MLCT_{hi}$; with energy difference $\Delta h\nu_{max}$) found in the ambient absorption spectra of $[Ru(NH_3)_4(Y\text{-}py)_2]^{2+}$ complexes are largely attributable HOMO→LUMO and HOMO→LUMO+1 transitions, respectively, where the LUMO corresponds to the antisymmetric and the LUMO+1 to the symmetric combination of weakly mixed pyridyl acceptors. The properties of the closely related $[Ru(NH_3)_4bpy]^{2+}$ complex are consistent with strong mixing between its pyridyl moieties. In contrast, the similar partly resolved $MLCT_{lo}$ and $MLCT_{hi}$ absorption envelopes found for $[Ru(L)_2(bpy)_2]^{m+}$ complexes are largely attributable to the energy differences of donor orbitals.

That the calculations using the B3PW91 functionals with the SDDall basis set[64] model the energies and bandshapes of the lowest energy MLCT absorption envelopes of most of these complexes reasonably well indicates that (1) the LUMO and LUMO+1 orbitals of the DA_2 complexes with C_2 symmetry usually correspond to the antisymmetric and symmetric combinations of independent diabatic pyridyl or bipyridyl acceptor ligand orbitals; (2) in some of the complexes the low energy HOMO→LUMO MLCT transitions are too weak to be observed in ambient spectra; (3) in many complexes, the observed MLCT transitions involve the lower energy dπ donor orbitals (HOMO-1 and/or HOMO-2). Thus, the interpretation of these absorption spectra generally requires consideration of all of the dπ(Ru) orbitals. The ancillary ligands are effective in tuning both the MLCT excited states energies and the oscillator strengths of the corresponding transitions in these complexes through their effects on both the metal dπ orbital energies and the spatial distributions of the orbital densities. Donor/acceptor spatial orbital overlap has long been regarded as an important feature of charge transfer spectroscopy,[20] but the unique feature of these complexes is that the spatial overlap properties of the dπ(Ru) orbitals with the acceptor ligands vary appreciably in the different classes and with the different ancillary ligands. This results in (1) large variations in the oscillator strengths of the transitions with same orbital compositions in different complexes; and (2) correlated, appreciable variations in ground state/excited state configurational mixing.

While all the MLCT transitions of these complexes should correlate in some way with $F\Delta E_{1/2}$, both the experimental observations and the computational modeling indicate that the most chemically relevant transitions of $[Ru(L)_2(bpy)_2]^{m+}$ and $[Ru(L)_4bpy]^{m+}$ complexes have relatively small oscillator strengths and appreciably lower energies than the dominant absorption maxima that are commonly used in such contexts. The correlations of either the experimental or the DFT-modeled transition energies with $F\Delta E_{1/2}$ are relatively shallow consistent with appreciable Ru/bpy configurational mixing.

Acknowledgment. This work was funded in part by the Division of Chemical Sciences, Geosciences, and Biosciences, Office of Basic Energy Sciences of the U.S. Department of Energy through Grants DE-FG02-88ER13944 and DE-FG02-09ER16120 and in part by the Office of the Vice President for Research of Wayne State University.

Supporting Information Available: Synthesis of bis-acac ruthenium bipyridine complexes; comparison of observed and calculated (from rR parameters) $[Ru(NH_3)_4bpy]^{2+}$ absorption spectrum; computational basis sets used; MLCT absorption spectra of complexes; solvent variations of the lowest energy MLCT absorption bands for some complexes; electrochemical data; comparison of computational methods; solvent contributions to $[Ru(bpy)_2Cl_2]$ orbital energies; computed HOMOs and LUMOs for several $[Ru(L)_2(bpy)_2]^{m+}$ complexes; computed HOMOs and LUMOs for $[Ru(NH_3)_4(Y\text{-}py)_2]^{2+}$ and $[Ru(acac)_2bpy]^+$ complexes; comparison of calculated orbital energies for different bis-bpy complexes; calculated orbital compositions; comparison of the observed and calculated MLCT spectra of some complexes; composition of calculated transitions; correlation of calculated LUMO−HOMO energy differences with $F\Delta E_{1/2}$ for bis bpy complexes; perturbation theory-based three state model of DA_2 complexes; comparison of the calculated HOMO/LUMO MLCT transition to $F\Delta E_{1/2}$. This material is available free of charge via the Internet at http://pubs.acs.org.

(89) Odongo, O. S.; Allard, M. M.; Schlegel, H. B.; Endicott, J. F. *Inorg. Chem.* 2010, submitted for publication.